ADVANCED FUNCTIONAL MATERIALS
www.afm-journal.de

Materials Views
www.MaterialsViews.com

Formation and Control of Ultrasharp Metal/Molecule Interfaces by Controlled Immobilization of Size-Selected Metal Nanoclusters onto Organic Molecular Films

*Masato Nakaya, Takeshi Iwasa, Hironori Tsunoyama, Toyoaki Eguchi, and Atsushi Nakajima**

The formation of metallic layers on ultrathin molecular films via a well-controlled interface is essential for constructing organic nanodevices composed of metal/molecule/metal sandwich junctions. The scanning tunneling microscopy and spectroscopy studies demonstrate that an ultrasharp metal/molecule interface is realizable by depositing size-selected Ag nanoclusters (Ag_n) from the gas phase on few-layer films of C_{60} molecules. It is also demonstrated that Ag_n nanoclusters can be immobilized on monolayer films of oligothiophene molecules via C_{60} molecules, although they three-dimensionally aggregate on bare oligothiophene films. It is also shown that electrons and holes are injected into the topmost layer of C_{60} films via the Ag_n/C_{60} interface. Moreover, the barrier height for carrier injection at the Ag_n/C_{60} interface can be modified depending on the size of Ag_n nanoclusters and the kinetic energy during the deposition. The present results demonstrate that the controlled immobilization of metallic nanoclusters on molecular films can be used as a fabrication technology for metal/molecule/metal junctions.

1. Introduction

The construction of ultrathin metal/molecule/metal sandwich junctions using few-layer organic thin films is a critical requirement toward achieving the ultimate miniaturization and low-energy consumption of practical organic nanodevices possessing functionalities such as electroluminescence, electrical switching, charge storage, and chemical sensing.[1–6] A key factor in realizing the high-performance operation of such nanodevices is the controlled injection of charged carriers into molecular films of an active element, which strongly depends on the geometrical sharpness and energy-level alignment at the molecule/metal and metal/molecule interfaces.[7,8] Although the alternate stacking of organic molecules and metal atoms by physical vapor deposition is widely accepted as a practical method of fabricating heterojunctions, it is difficult to avoid the penetration of deposited metal atoms into molecular films,[8–12] which leads to the undesirable modification of molecules near the metal/molecule interface[8,10–12] or the formation of conductive filaments causing short circuits between the electrodes.[13] To exclude such uncontrollable factors in the functionality of metal/molecule junctions, a considerable number of studies have been conducted to find appropriate combinations of metallic elements and molecular films from the viewpoints of chemical reactivity and electronic interactions.[7,8,12,14]

On the other hand, in heterojunctions composed of a single or a few molecules sandwiched by two metallic electrodes, metal particles with sizes of 10–100 nm serve as contact points for the molecules.[15] Although this method enables us to realize stable and abrupt metal/molecule interfaces, it is generally difficult to fabricate dense metallic layers that widely interconnect with molecular films using metal particles owing to the large size mismatch between such metal particles and nanoscale functional molecules. This is directly related to the realization of efficient charge injection into molecular films. In contrast, it has been widely demonstrated that diverse metallic nanoclusters can be synthesized in the gas phase with atomic-scale size controllability ranging in scale from single atoms to a size of more than several nanometers.[16] In addition, since metallic nanoclusters also exhibit tunable physical and chemical properties depending on their size,[16–19] it is expected that the use of size-controlled metallic nanoclusters as a component of metal/molecule junctions will lead to the realization of controllable electrode/molecule interfaces with a wide range of geometries and electronic properties. The key technology toward this end is the immobilization of metal nanoclusters on ultrathin molecular films while maintaining the geomety and electronic properties of the nanoclusters and the underlying molecular films. In this sense, extensive knowledge of the physical properties

Dr. M. Nakaya, Dr. T. Iwasa, Dr. H. Tsunoyama, Dr. T. Eguchi, Prof. A. Nakajima
Nakajima Designer Nanocluster Assembly Project
ERATO, JST, KSP, 3–2–1 Sakado,
Takatsu-ku, Kawasaki, 213–0012, Japan
E-mail: nakajima@chem.keio.ac.jp
Dr. M. Nakaya, Dr. T. Iwasa, Dr. H. Tsunoyama, Dr. T. Eguchi, Prof. A. Nakajima
Department of Chemistry
Faculty of Science and Technology
Keio University
3–14–1 Hiyoshi, Kohoku-ku, Yokohama, 223–8522, Japan

DOI: 10.1002/adfm.201302187

© 2013 WILEY-VCH Verlag GmbH & Co. KGaA, Weinheim

of nanocluster/molecule junctions will be gained by evaluating these junctions at the molecular and atomic scales.

Here, we have investigated the geometry and electronic properties of metal/molecule junctions constructed by depositing size-selected Ag nanoclusters (Ag_n; n = 7, 13, and 55) from the gas phase on ultrathin films of C_{60} and oligothiophene molecules using scanning tunneling microscopy and spectroscopy (STM/STS). In contrast to Ag atoms deposited on ultrathin C_{60} films, which aggregate into large islands at room temperature (RT) and encroach on the C_{60} films, the deposited Ag_n nanoclusters are stably immobilized at RT on the surface of the films and can densely cover the surface. The STM and STS results indicate that atomically abrupt interfaces are formed between Ag_n nanoclusters and C_{60} films, which enable the injection of electrons and holes into the topmost layer of the films. The barrier height for carrier injection changes depending on the size of nanoclusters and the kinetic energy of nanoclusters during the deposition. We have also demonstrated that the Ag_n nanoclusters can be immobilized on monolayer films of oligothiophene molecules via C_{60} molecules, although Ag_n nanoclusters three-dimensionally aggregate on bare oligothiophene thin films.

2. Results and Discussion

2.1. Formation of Ag_n/C_{60} Heterojunctions

Ultrathin C_{60} films were grown on a Si(111)$\sqrt{3}\times\sqrt{3}$R30°-Ag [referred to as Si(111)$\sqrt{3}$-Ag hereafter] substrate. Ag_n cations were deposited on the C_{60} films by applying a negative bias voltage (V_{sub}) to the substrate to collect Ag_n cations efficiently, which imparts a kinetic energy of $E_k = V_{sub}/n$ (eV/atom) to the cations. **Figures 1**a,b show STM images taken at RT after depositing Ag_{55} cations with E_k of ≈0.09 eV/atom on C_{60} films with coverages of 1.7 and 3.5 monolayers (ML), respectively: the former surface is composed of a monolayer and bilayer of C_{60}, whereas the latter consists of a trilayer and tetralayer. It can be seen that dot-shaped structures are formed on both surfaces. The histograms of dot heights (h_d) measured on both surfaces show a main peak centered at ≈1.2 nm, as indicated in Figure 1d,e. This value is in good agreement with the theoretical heights of icosahedral Ag_{55} nanocluster, which ranges from 1.17 to 1.4 nm depending on the orientation (Figure 1c). In addition, each dot is smooth and spherical without an internal structure, as shown in the magnified image (inset in Figure 1b). These results indicate that most of the dots consist of individual Ag_{55} nanoclusters immobilized on C_{60} films without obvious aggregation, fragmentation, or the formation of two-dimensional assemblies of multiple Ag_{55} nanoclusters.

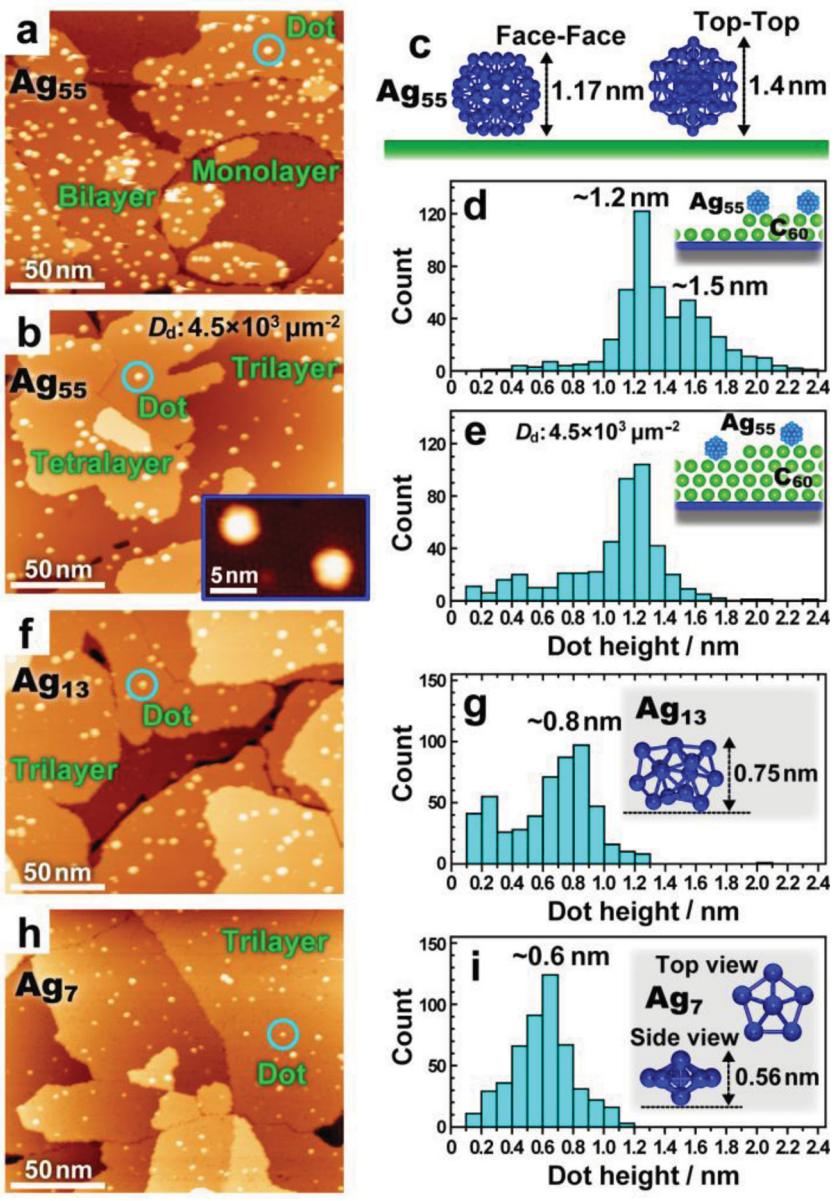

Figure 1. Soft landing of Ag_{55}, Ag_{13}, and Ag_7 nanoclusters on ultrathin C_{60} films. STM images of a) bilayer/monolayer and b) trilayer/tetralayer of C_{60} taken after the soft landing of Ag_{55} nanoclusters. The inset in (b) is a magnified image of two dots. c) Theoretical height of icosahedral Ag_{55}. d,e) Histograms of dot heights measured on surfaces shown in (a) and (b), respectively. f) STM image and g) height histogram of dots measured on C_{60} multilayer after depositing Ag_{13} cations. The inset in (g) is a geometrical model of Ag_{13} nanocluster and its theoretical height. h) STM image and i) height histogram of dots measured on C_{60} multilayer after depositing Ag_7 cations. The inset in (i) shows a geometrical model of Ag_7 nanocluster and its theoretical height. The imaging conditions are V_{tip} = –1 V and I_t = 7 pA for (a), V_{tip} = –2 V and I_t = 10 pA for (b,f,h), and V_{tip} = –1.2 V and I_t = 10 pA for the inset in (b). The scan area of (a,b,f,h) is 180 nm × 150 nm.

© 2013 WILEY-VCH Verlag GmbH & Co. KGaA, Weinheim

Note that the dot density on the C_{60} monolayer is much lower than that on the coexisting bilayer, as shown in Figure 1a. In connection with this, a previous study on Ag_{309} nanoclusters deposited on C_{60} monolayers formed on a Au(111) substrate proved that the attractive force acting between the nanoclusters and substrate causes the disintegration of the nanoclusters,[20] which leads to the formation of Ag monolayer islands at the C_{60}/substrate interface. In the present case, there is no geometrical modulation at the surfaces originating from Ag islands. A possible reason for this is that smaller clusters or atoms that are segregated from the Ag_{55} nanoclusters on the monolayer diffuse across the surface and coalesce with the Ag_{55} nanoclusters already adsorbed on the bilayer. This is corroborated by the height distribution of dots formed on the surface with the coexisting C_{60} monolayer and bilayer (Figure 1d), which shows a small number of dots with h_d of ≈1.5 nm higher than the expected value of ≈1.2 nm for Ag_{55} nanoclusters.

It is also possible to immobilize smaller Ag_n nanoclusters onto C_{60} films at RT. Figures 1f and 1h show STM images taken after depositing Ag_{13} and Ag_7 cations on C_{60} multilayers with E_k of ≈0.38 eV and ≈0.71 eV, respectively. Dot-shaped structures are created on the both surfaces similarly to the case of Ag_{55} deposition, although the dots are smaller. The dot height histograms measured on the Ag_{13}- and Ag_7-deposited surfaces (Figure 1g,i) show a single peak centered at ≈0.8 nm and ≈0.6 nm, respectively. They are in good agreement with the theoretical heights of 0.75 nm and 0.56 nm calculated for individual neutral Ag_{13} and Ag_7 nanoclusters, respectively. The successful immobilization of Ag_{55}, Ag_{13}, and Ag_7 nanoclusters without significant disorganization or deformation is consistent with the fact that the values of E_k of the deposited Ag_{55} (≈0.09 eV/atom), Ag_{13} (≈0.38 eV/atom), and Ag_7 (≈0.71 eV/atom) cations are sufficiently smaller than the interatomic binding energies of Ag_{55} (≈2.1 eV), Ag_{13} (≈1.7 eV), and Ag_7 (1.5–1.71 eV) nanoclusters, respectively,[18,21,22] namely, the soft landing of nanoclusters[20,23–26] is achieved.

The individuality of each nanocluster was also preserved at a higher dot density. **Figure 2**a shows an STM image taken on a Ag_{55}-deposited C_{60} multilayer with a dot density of 4.3 × 10^4 dots/μm^2. The coverage is ten times higher than that in the initial stage shown in Figure 1b; nevertheless, the surface is uniformly covered with dots without significant aggregation. It is confirmed that the main peak in the height histogram of the dots remains at the theoretical height of ≈1.2 nm for Ag_{55} nanocluster for a dot density of at least up to 2.3 × 10^4 dots/μm^2 as shown in Figure 2b. This suggests that, after soft landing, the Ag_{55} nanoclusters are immobilized on the C_{60} films after little or no surface migration, which suppresses the coalescence of the nanoclusters. Comparing the histograms shown in Figures 1e,2b, the fraction of dots higher than the theoretical height of Ag_{55} increases with increasing dot density on the surface, which is considered to be due to that Ag_{55} nanoclusters occasionally aggregate via the direct adsorption of deposited Ag_{55} nanoclusters onto preexisting nanoclusters.

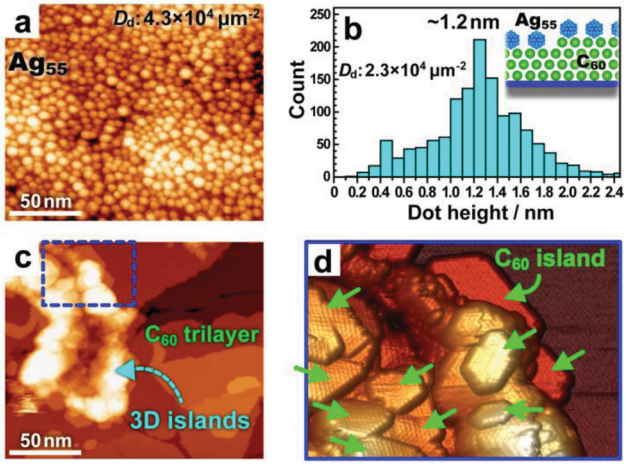

Figure 2. Formation of metallic layers on ultrathin C_{60} films by soft landing of Ag_{55} nanoclusters and physical vapor deposition of Ag atoms. a) STM image and b) height histogram of dots measured on C_{60} multilayer densely covered with dots after soft landing of Ag_{55} nanoclusters. c) STM images of C_{60} multilayer film taken after physical vapor deposition of Ag atoms at RT. The deposition rate was ≈0.05 ML/min. d) Magnified three-dimensional image of the region surrounded by the dashed blue line in (c). The imaging conditions of all STM measurements are V_{tip} = –2 V and I_t = 10 pA. The scan area of (a,c) is 180 × 150 nm^2.

Such soft landing of Ag_n nanoclusters is advantageous for fabricating a uniform metallic layer on ultrathin C_{60} films over conventional methods. For instance, Figure 2c shows STM images of a C_{60} multilayer film taken after depositing ≈0.15 ML (≈2 × 10^6 atoms/μm^2) of Ag atoms at RT. After depositing Ag

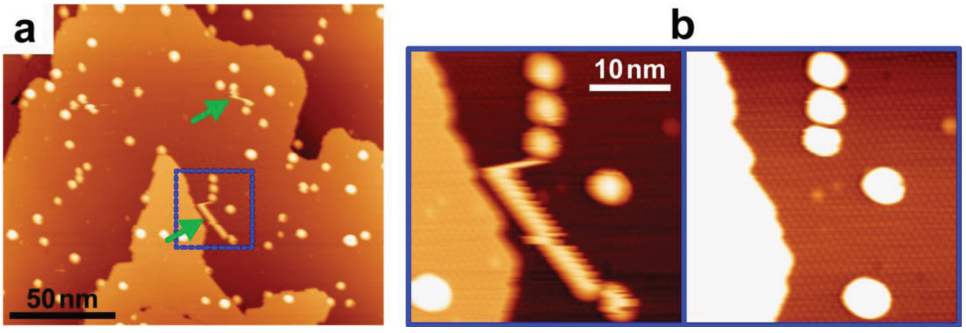

Figure 3. STM-induced lateral movement of Ag_{55} nanoclusters. a) STM image of C_{60} multilayer taken after depositing Ag_{55} with E_k of ≈0.09 eV/atom. The left panel in (b) shows a magnified image of the region surrounded by blue lines in (a), which shows the trace of the multistep displacement of a cluster induced by the STM scan. The right panel in (b) is an STM image taken in the same region as the left panel after inducing the nanocluster movement. All STM images were taken at RT under the conditions of V_{tip} = –2 V and I_t = 10 pA.

© 2013 WILEY-VCH Verlag GmbH & Co. KGaA, Weinheim

atoms, large three-dimensional islands were sparsely formed on the surface, as a result of the extensive migration of Ag atoms. Furthermore, there are many small C_{60} islands in the vicinity and on the surface of the Ag islands, as indicated by green arrows in the magnified image shown in Figure 2d. They are considered to originate from the rearrangement of C_{60} molecules induced by the encroachment of Ag islands on the C_{60} films. The size and density of the Ag islands increase with increasing number of deposited Ag atoms, which causes further destruction of the C_{60} films. In contrast, marked morphological changes of the C_{60} films, such as the formation of small C_{60} islands and cracks, are not induced by the soft landing of Ag_n nanoclusters even when the nanoclusters densely cover the C_{60} films, as shown in Figure 2a and the Supporting Information. This strongly indicates that the deposited Ag_n nanoclusters do not penetrate into the C_{60} films and induce any rearrangement of C_{60} molecules. In particular, the latter means that the Ag_n nanoclusters weakly interact with C_{60} molecules at Ag_n/C_{60} interfaces.

The weak interaction between Ag_n nanoclusters and C_{60} molecules at Ag_n/C_{60} interfaces is supported by the results of the STM-induced lateral manipulation of Ag_n nanoclusters adsorbed on C_{60} films. **Figure 3**a shows an STM image of a C_{60} multilayer film taken after depositing Ag_{55} nanoclusters with E_k of ≈0.09 eV/atom. The STM imaging was carried out by raster-scanning the STM tip over the surface in the downward direction at RT. Although Ag_n nanoclusters that are immobilized on the C_{60} multilayer are sufficiently stable at RT as mentioned above, scanning the STM tip over the Ag_n nanoclusters occasionally induces their lateral displacement on the surface, for example, the nanoclusters indicated by green arrows in Figure 3a. Such displacement tends to become more frequent with decreasing tunneling gap. The left and right panels in Figure 3b show STM images obtained during and after the STM-induced nanocluster displacement, respectively. In this example, multistep displacements occurred in the downward direction during the downward STM scan, making it possible to visualize the track of nanocluster movement. Interestingly, there is no evident change in the C_{60} film after manipulating the nanoclusters, as shown in the right panel in Figure 3b, indicating that the Ag_n nanoclusters are immobilized on the C_{60} films without strong interactions such as the formation of rigid covalent bonds or C_{60}-Ag complexes.[27] Similar manipulation of metal nanoclusters has been reported for Pd nanoclusters weakly adsorbed on a graphene surface.[26] In addition, the noncovalent interaction between C_{60} molecules and Ag_n nanoclusters was also observed in [Ag_n-C_{60}] cations created in the gas phase.[28]

2.2. Charged-Carrier Injection at Ag_n/C_{60} Heterointerface

On the basis of the STS results, the characteristics of charged-carrier injection at Ag_n/C_{60} heterointerfaces are discussed. **Figure 4**a,d show the STS spectra taken on dots created by the soft landing of Ag_{55} cations with E_k of ≈0.09 eV/atom on a C_{60} bilayer and a C_{60} trilayer, respectively. The dI/dV spectra at positive (negative) tip bias voltages (V_{tip}) probe the filled (empty) states of a sample. In the Ag_{55}/bilayer, two dI/dV peaks of filled (A) and empty (B) states are observed at V_{tip} of approximately +1.4 V and –0.9 V, respectively. On the other hand, in the STS spectrum taken on the Ag_{55}/trilayer, dI/dV peaks appear at +1.3 V (C) and –1.4 V (D). The peak positions are more dependent on the thickness of the C_{60} film than on the size of the

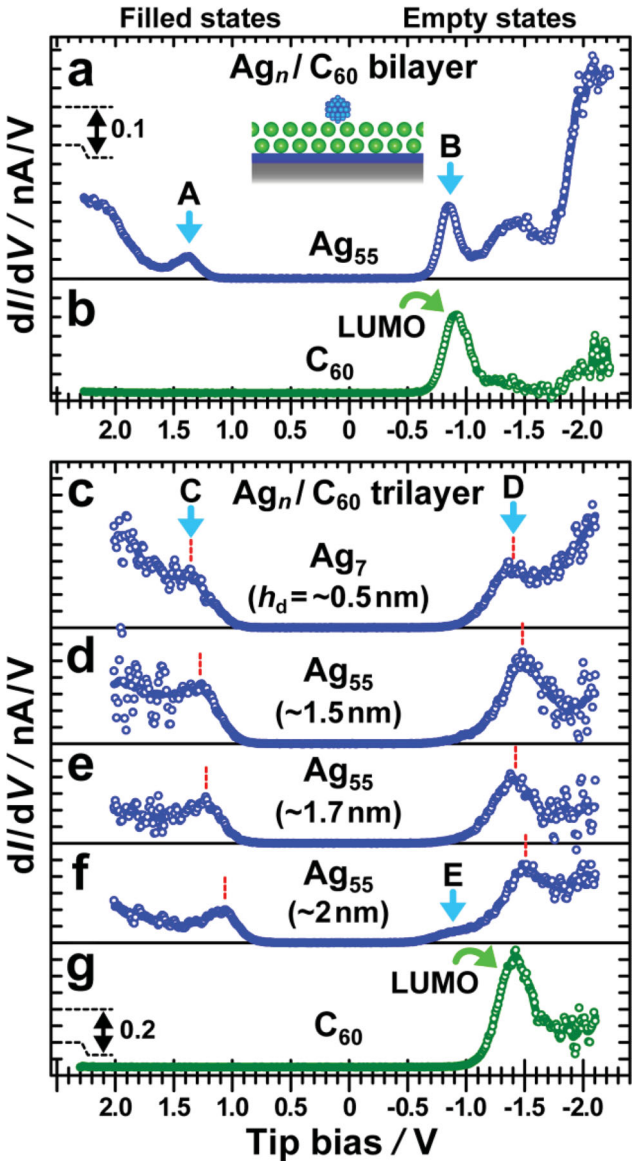

Figure 4. STS measurements on Ag_n/C_{60} junctions formed by soft landing of Ag_n nanoclusters. dI/dV spectra of a) single Ag_{55} nanocluster and b) bare C_{60} molecules in the C_{60} bilayer. dI/dV spectra of the dots created by depositing c) Ag_7 and d–f) Ag_{55} nanoclusters with E_k of 0.09 eV/atom and g) of bare C_{60} molecules in the C_{60} trilayer. d,e,f) Spectra of larger dots with h_d of ≈1.5, ≈1.7, and ≈2.0 nm, respectively. Each dI/dV datum was numerically derived from the respective tunneling I–V curve obtained by averaging almost one hundred original curves. The original tunneling I–V curves were measured on a surface with coexisting Ag_n nanoclusters and bare C_{60} molecules with a spatial resolution of ≈0.13 nm by current imaging tunneling spectroscopy. The set points of the I–V measurements are V_{tip} = –1.3 V and I_t = 60 pA for (a,b) and V_{tip} = –1.4 V and I_t = 80 pA for (c–g).

© 2013 WILEY-VCH Verlag GmbH & Co. KGaA, Weinheim

nanoclusters, as can be seen by comparing the spectra of the Ag_7/trilayer (Figure 4c). Note that the changes in the spectral features are also observed for much larger nanoclusters, as will be discussed later. The energy gaps of 2.3 eV for the Ag_{55}/bilayer and 2.7 eV for the Ag_7/trilayer and Ag_{55}/trilayer observed in Figure 4a,c,d, respectively, are clearly larger than the energy gap between the highest occupied molecular orbital (HOMO) and lowest unoccupied molecular orbital (LUMO) of an isolated Ag_n nanocluster, which is expected to be about 0.3 eV and below 0.1 eV for Ag_7 and Ag_{55}, respectively.[18,22] This fact suggests that the observed dI/dV peaks do not reflect the electronic states of Ag_n nanoclusters but the barrier height for carrier injection at the Ag_n/C_{60} interfaces, as will be discussed next.

An interesting point is that the first dI/dV peaks in the empty states of the Ag_n/bilayer (B) and Ag_n/trilayer (D) are observed at nearly identical energies to those of the LUMO of C_{60} molecules in the bilayer (Figure 4b) and trilayer (Figure 4g), respectively. This strongly indicates that the positions of peaks B and D correspond to the barrier height of electron injection at each Ag_n/C_{60} interface, namely, the tunneling current at a negative V_{tip} is generated by the injection of electrons from the STM tip into the LUMO of C_{60} molecules in the topmost layer through Ag_n, as illustrated in the schematic potential diagrams of the tip/gap/Ag_n/C_{60}/substrate (**Figure 5**c).

Turning to the filled states, one can find a significant difference between the spectra obtained on the bare C_{60} molecules and soft-landed Ag_n nanoclusters. On the C_{60} molecules, there are no significant peaks in the STS spectra within the bias voltage range from 0 to +2.3 V, as shown in Figure 4b,g, although it has been reported that the HOMO of C_{60} molecules in a bilayer and trilayer appear at ≈2.1 eV below E_F in the case of two-photon photoemission (2PPE) spectroscopy.[29] This is because the strong electric field generated in the tunneling gap beneath an STM tip induces a downward energy shift of the HOMO of C_{60} molecules in the topmost layer,[30] as schematically illustrated in Figure 5b, which inhibits efficient hole injection into C_{60} films. In contrast, the dI/dV peak in the filled states is clearly observed on Ag_n/C_{60}, as shown in Figures 4a,c,d, indicating that the injection of holes into the C_{60} films can be realized through the immobilized Ag_n. On the other hand, it is known that, in conventional metal/C_{60} junctions, electrons are also injected preferentially into C_{60} films rather than holes, because the HOMO of C_{60} molecules is located at a much lower energy than the E_F of metals in the junctions owing to the large ionization potential of C_{60}.[31,32] In contrast, the Ag_n/C_{60} junction constructed by the soft landing of Ag_n nanoclusters on a C_{60} trilayer film enables the injection of electrons and holes with similar barrier heights of 1.3–1.4 eV, namely, ambipolar carrier injection[31,33] is possible. Note that the injection barrier of the holes is lower than that expected from the energy level of the HOMO of C_{60} molecules in the trilayer, which appears at approximately ≈2.1 eV below E_F.[29] This suggests that the hole injection into the C_{60} films has been realized not through the pristine HOMO of the C_{60} molecules in the topmost layer but through the hybridized molecular orbitals locally formed at the interface between Ag_n nanoclusters and their neighboring C_{60} molecules, as indicated in the schematic potential diagrams (Figure 5d).

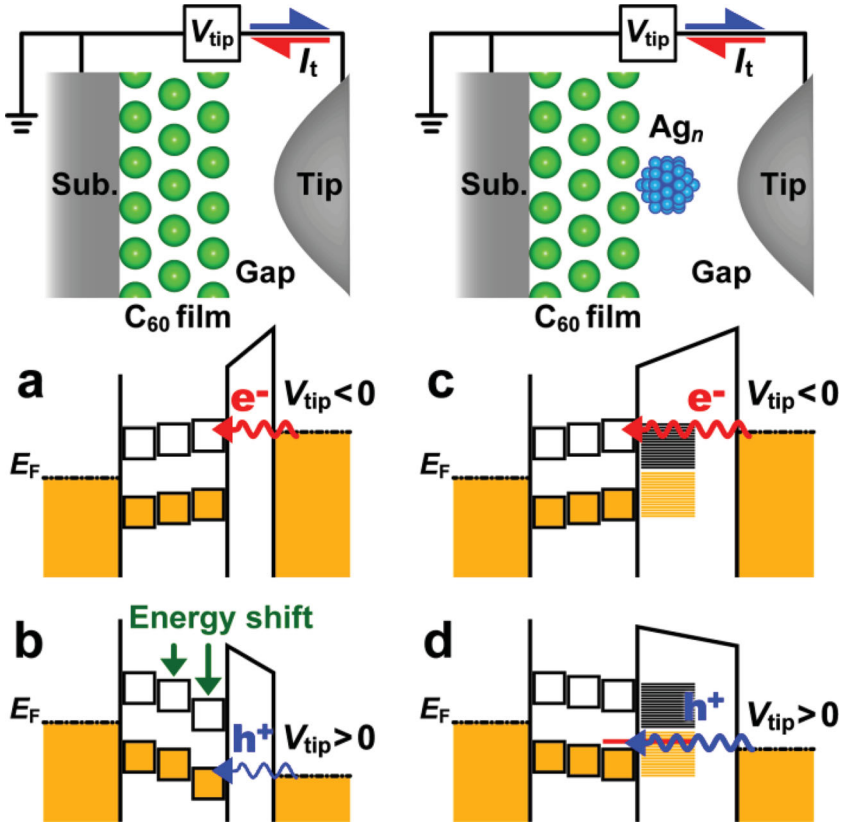

Figure 5. Schematic side view and potential diagrams of tip/gap/C_{60}/substrate junction while applying a) negative and b) positive bias voltages to the tip (V_{tip}). Schematic side view and potential diagrams of tip/gap/Ag_n/C_{60}/substrate junction while applying c) negative and d) positive values of V_{tip}.

It is found that the barrier height for carrier injection changes depending on the size of the nanoclusters. Figures 4e,f show the STS spectra taken on large dots with h_d of ≈1.7 nm and ≈2 nm, respectively, which are occasionally created by the aggregation of the soft-landed Ag_{55} nanoclusters on the C_{60} trilayer at a higher cluster coverage, as mentioned above. By comparing the STS spectra of the clusters of different sizes shown in Figures 4c–f, it is clear that the first dI/dV peak in the filled states (C) appears at a lower V_{tip} with increasing cluster size, that is, the barrier height of hole injection decreases with increasing cluster size, which markedly occurs for dots with h_d of ≈2 nm. In the empty states, although there is no evident change in the energy position of the first dI/dV peak (D), a shoulderlike feature (E) appears at approximately –0.9 V as shown in Figure 4f, which also becomes more pronounced with increasing cluster size and contributes to the reduction in the barrier height for electron injection at the Ag_n/C_{60} interface. The electronic state E is

© 2013 WILEY-VCH Verlag GmbH & Co. KGaA, Weinheim

more clearly observed in the STS measurement at the Ag_n/C_{60} junction created by depositing Ag_n cations with a higher E_k, as will be shown next, which is considered to originate from the reconfiguration of the electronic structure of C_{60} molecules beneath the Ag_n nanocluster owing to the strong interaction at the Ag_n/C_{60} interface, as discussed below.

The barrier height for carrier injection at the Ag_n/C_{60} interface can also be modified by controlling E_k for Ag_n cations during the deposition. **Figure 6**a shows the STS spectrum of the dots created by depositing Ag_{55} cations on a C_{60} trilayer with an intentionally increased E_k of ≈1.7 eV/atom, which is almost 20 times larger than that used to obtain the STS spectra in Figures 4a,d. The peak positions in the filled (F) and empty (G) states indicate that the injection barriers of holes and electrons at the Ag_{55}/C_{60} interface are 1.0 and 0.9 eV, respectively, which are smaller than those for the soft-landed Ag_{55} nanoclusters shown in Figure 4d and almost identical to thse of the large clusters shown in Figure 4f.

It can be considered that the reduction in the height of the injection barriers at the Ag_n/C_{60} junction is associated with the modification of the interface structure. The red and blue histograms in Figure 6c show the height distributions of dots created by depositing Ag_{55} cations with higher (≈1.7 eV/atom) and lower (≈0.09 eV/atom) E_k, which were measured on the surfaces shown in Figures 6d and 6e, respectively. The histograms clearly show that the dot height decreases with increasing E_k, indicating that the deposited Ag_{55} nanoclusters disintegrated into smaller clusters on the surface, namely, the hard landing of nanoclusters occurred.[23,24] The dots created by hard landing are categorized into two types on the basis of their heights h_d of ≈0.4 nm and ≈0.7 nm, as seen in the red histogram in Figure 6c. The decreased height of the injection barriers was mainly measured on dots with the smaller h_d. Interestingly, the C_{60} molecules around the smaller dots exhibit a slightly brighter contrast in the STM image than those far from the dots (e.g., see the inset in Figure 6d), which is not observed for the dots created by soft landing (Figure 6e). This indicates that the C_{60} molecules in the vicinity of the smaller dots are modified electronically and/or geometrically, and also suggests that the electronic/geometric structures at the Ag_n/C_{60} interface are different from those in the case of soft landing, for instance, the formation of Ag-C_{60} complexes occurs at the interface. This consideration is supported by the fact that the above-mentioned STM-induced lateral movement hardly occurs for the disintegrated smaller dots created by hard landing compared with the soft-landed ones, which suggests the strong interaction between the hard-landed nanoclusters and C_{60} films. The analogy between the changes in the positions of the peaks in the STS spectra depending on the size of nanoclusters (Figure 4c–f) and on the deposition energy (Figures 4d,6a) implies that a similar intereaction partially occurs at the interface of large nanoclusters.

The formation of metal-C_{60} complexes has been widely demonstrated by the chemical doping of alkali metals into C_{60} films.[34] In metal-C_{60} complexes, electron donation from metal atoms to C_{60} molecules induces a marked upward shift in E_F or an increase in the width of the LUMO band.[34] In addition, it is also expected that midgap states between the HOMO and LUMO are induced in C_{60} molecules covalently bound to metallic elements, as reported for C_{60} molecules chemisorbed

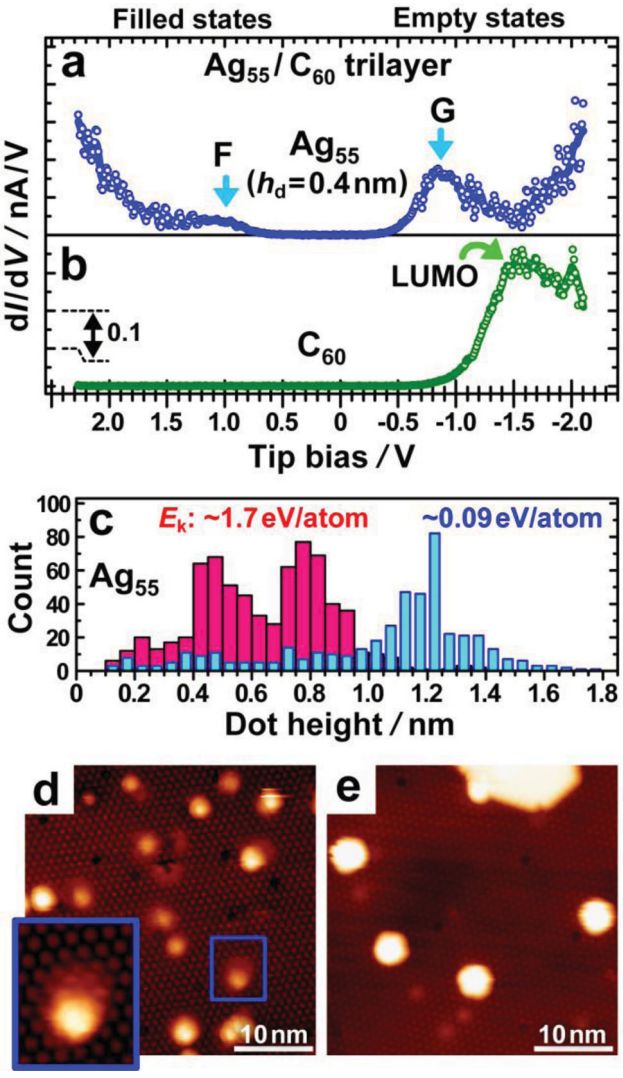

Figure 6. Ag_n/C_{60} junctions formed by hard landing of Ag_n nanoclusters. d*I*/d*V* spectra of a) dots and b) bare C_{60} molecules in C_{60} trilayer. The dots were created by depositing Ag_{55} cations with E_k of ≈1.7 eV/atom. The conditions for the *I*–*V* measurement are V_{tip} = –1.5 V and I_t = 80 pA. c) Histograms of dot heights measured on C_{60} films after depositing Ag_{55} cations with E_k of ≈1.7 eV/atom (red) and ≈0.09 eV/atom (blue). STM images (40 nm × 40 nm) of the C_{60} trilayer after depositing Ag_{55} cations with E_k of d) ≈1.7 eV/atom and e) ≈0.09 eV/atom. The imaging conditions are V_{tip} = –1.7 V and I_t = 10 pA for (d) and V_{tip} = –1.2 V and I_t = 10 pA for (e).

on solid surfaces.[35] These marked electronic modifications of C_{60} molecules could cause the reduction in barrier height for carrier injection at the Ag_n/C_{60} interface, although further studies of the geometry and energy-level alignment at the interface are needed for detailed understanding of the barrier height modification.

So far, we have demonstrated that a metallic layer can be formed on ultrathin C_{60} films via a controlled interface by the controlled deposition of size-selected Ag_n nanoclusters. To widely use this methodology to construct organic nanodevices, it is better to immobilize metallic nanoclusters onto various

© 2013 WILEY-VCH Verlag GmbH & Co. KGaA, Weinheim

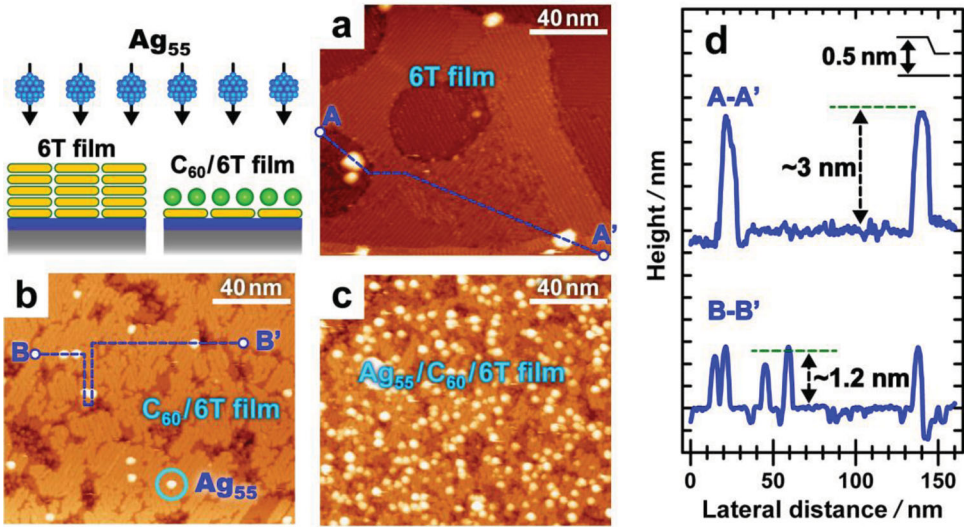

Figure 7. Immobilization of Ag_{55} nanoclusters onto ultrathin films of oligothiophene molecules. STM images of a) 6T multilayer (pentalayer and hexalayer) and b) C_{60}/6T structures taken after depositing Ag_{55} cations with E_k of ≈0.09 eV/atom. c) STM image of C_{60}/6T structures densely covered with Ag_{55} nanoclusters. d) Cross-sectional line profiles taken along line segments A-A' (upper) and B-B' (lower) in (a,b), respectively. The imaging conditions are $V_{tip} = -1.2$ V and $I_t = 10$ pA for (a), $V_{tip} = -2$ V and $I_t = 5$ pA for (b), and $V_{tip} = -1.7$ V and $I_t = 10$ pA for (c). The scan area of (a,b,c) is 150 nm × 130 nm.

organic thin films and nanostructures. From this perspective, we have investigated the immobilization of Ag_n nanoclusters onto thin films of α-sexithiophene (referred to as 6T hereafter) molecules. In addition, Ag_n nanoclusters were also deposited onto stacking structures composed of monolayers of C_{60} and 6T molecules. The junction between donor-like 6T molecules[36] and acceptor-like C_{60} molecules[32,37] is expected to behave as the active element of an ultrathin rectifier diode. **Figure 7**a shows an STM image taken after depositing Ag_{55} cations onto a 6T multilayer, where a pentalayer and a hexalayer coexist, with E_k of ≈0.09 eV/atom. Although dot-shaped structures are formed on the Ag_{55}-deposited 6T film, the density of the dots is clearly lower than that on the Ag_{55}-deposited C_{60} films (e.g., Figure 1b). In addition, the height of the dots on the 6T films is ≈3 nm, which is obviously larger than the theoretical height of ≈1.2 nm for Ag_{55}, as shown in the cross-sectional line profile taken along line segments A-A' (upper curve in Figure 7d). These results clearly indicate that, on a bare 6T film, individual Ag_{55} nanoclusters are hardly immobilized and aggregate into larger clusters. It is also found that the aggregation of Ag_{55} nanoclusters becomes pronounced on the 6T monolayers, which results in the formation of large three-dimensional islands. This tendency can be markedly changed by functionalizing the surface of 6T films with C_{60} molecules: uniform dot-shaped structures with a height of ≈1.2 nm are created by depositing Ag_{55} cations on a 6T monolayer covered with ≈1 ML of C_{60} molecules, as shown in the STM image (Figure 7b) and cross-sectional line profile (lower curve in Figure 7d). Furthermore, the density of the dots on the C_{60}-modified 6T films increases with increasing number of Ag_{55} nanoclusters deposited, as shown in Figure 7c. On the basis of the present results, we consider that monolayers of various functional molecules can be covered by metallic nanoclusters via C_{60} molecules without disorganizing the molecular films, since surface functionalization using C_{60} molecules has been realized on various molecules, such as cyclothiophene, coronene, metal porphyrins and metal phthalocyanines.[38–43]

Our results show that C_{60} molecules can preferentially trap Ag_n nanoclusters, which may originate from the character of the chemical bond in C_{60} molecules. In connection with this, it has been reported that the Moiré pattern formed by graphene layers grown on a late-transition-metal substrate can be used as the template for the periodic arrangement of metal nanodots,[44] since the buckling of graphene layers permits the local rehybridization of C–C bonds from sp^2 to sp^3 and enhances their chemical reactivity. It can be considered that the sp^3-like character of C–C bonds in C_{60} molecules enables these molecules to more effectively react with metal nanoclusters than with oligothiophene molecules, which consist of two-dimensional sp^2-hybridized carbon atoms. A detailed understanding of the interaction between metallic nanoclusters and functional molecules based on the results of further experiments and theoretical calculations would provide guiding principles for the construction of metal/molecule/metal junctions using metallic nanoclusters.

3. Conclusions

We have demonstrated that well-controlled metal/molecule heterojunctions can be constructed by the controlled immobilization of size-selected Ag_n nanoclusters from the gas phase onto ultrathin films of C_{60} molecules. In such heterojunctions, electrons and holes can be precisely injected into the topmost C_{60} molecules in the thin films via an atomically abrupt Ag_n/C_{60} interface. The barrier height for carrier injection can be changed by controlling the size of nanoclusters and the kinetic energy during the deposition. It has also been demonstrated that Ag_n nanoclusters can be immobilized on monolayer films of oligothiophene molecules via C_{60}

© 2013 WILEY-VCH Verlag GmbH & Co. KGaA, Weinheim

molecules. We expect these findings to provide novel insights into the technology for constructing metallic electrodes on ultrathin films of various functional molecules via a well-defined and well-controlled interface, which is widely known as one of the key technologies for realizing future molecular nanodevices.[1–3,7,8,15] In addition, we also expect the present results to provide methodological insights not only into the fabrication of metal/molecule/metal junctions but also into the development of cluster-assembled materials constructed on molecular templates.[45,46]

4. Experimental Section

Experimental Method: Ultrathin C_{60} films with a well-ordered molecular arrangement were prepared by depositing an appropriate number of C_{60} molecules on a Si(111)$\sqrt{3}$-Ag surface in ultrahigh vacuum (UHV). Si(111)$\sqrt{3}$-Ag surfaces were prepared by depositing 1 ML (7.83×10^6 atoms/μm^2) of Ag atoms on a Si(111)7×7 surface at 600 °C. C_{60} molecules were deposited at RT by the thermal evaporation of C_{60} powder (purity: 99.95%) from a Ta crucible while maintaining a deposition rate of 0.03 ML/min, where 1 ML of C_{60} corresponds to 1.15×10^6 molecules/μm^2. 6T films were also prepared by depositing an appropriate number of 6T molecules on the Si(111)$\sqrt{3}$-Ag surfaces in UHV. 6T molecules were deposited at RT by the thermal evaporation of 6T powder from a Ta crucible while maintaining a deposition rate of 0.015 ML/min. Ag_n cations with various sizes were produced in a gas aggregation apparatus with a magnetron sputtering source and directed into a quadrupole mass spectrometer (Extrel, mass limit 16 000 amu) for size selection. The size-selected Ag_n cations were deposited on C_{60} films at ≈90 K at a typical rate of 1.3×10^3 ions/(μm^2 min). The samples were transferred into an analysis chamber equipped with a commercial STM unit (Omicron VT-AFM-XA50/500) while maintaining the UHV condition. All STM/STS experiments were performed at RT using an electrochemically etched W tip. STM images were analyzed using WSxM.[47]

Theoretical Method: The theoretical optimization of the geometries of neutral Ag_{55}, Ag_{13}, and Ag_7 nanoclusters was performed at the RI-BP86[48–50] level as implemented in TURBOMOLE 6.4[51] using the def-SV(P) basis sets[52] along with a scalar relativistic effective core potential.[53]

Supporting Information

Supporting Information is available from the Wiley Online Library or from the author.

Received: June 28, 2013
Revised: August 29, 2013
Published online: October 14, 2013

[1] J. E. Green, J. W. Choi, A. Boukai, Y. Bunimovich, E. Johnston-Halperin, E. Delonno, Y. Luo, B. A. Sheriff, K. Xu, Y. S. Shin, H.-R. Tseng, J. F. Stoddart, J. R. Heath, *Nature* **2007**, *445*, 414.
[2] Y. Yang, J. Ouyang, L. Ma, R. J.-H. Tseng, C.-W. Chu, *Adv. Funct. Mater.* **2006**, *16*, 1001.
[3] R. L. McCreery, A. J. Bergren, *Adv. Mater.* **2009**, *21*, 4303.
[4] Z. J. Donhauser, B. A. Mantooth, K. F. Kelly, L. A. Bumm, J. D. Monnell, J. J. Stapleton, D. W. Price Jr., A. M. Rawlett, D. L. Allara, J. M. Tour, P. S. Weiss, *Science* **2001**, *292*, 2303.
[5] N. Sanetra, Z. Karipidou, R. Wirtz, N. Knorr, S. Rosselli, G. Nelles, A. Offenhaeusser, D. Mayer, *Adv. Funct. Mater.* **2012**, *22*, 1129.
[6] V. Iancu, S.-W. Hla, *Proc. Natl. Acad. Sci.* **2006**, *103*, 13718.
[7] H. Ishii, K. Sugiyama, E. Ito, K. Seki, *Adv. Mater.* **1999**, *11*, 605.
[8] J. Hwang, A. Wan, A. Kahn, *Mater. Sci. Eng. R* **2009**, *64*, 1.
[9] F. Faupel, R. Willecke, A. Thran, *Mater. Sci. Eng.* **1998**, *R22*, 1.
[10] A. V. Walker, T. B. Tighe, O. M. Cabarcos, M. D. Reinard, B. C. Haynie, S. Uppili, N. Winograd, D. L. Allara, *J. Am. Chem. Soc.* **2004**, *126*, 3954.
[11] G. L. Fisher, A. V. Walker, A. E. Hooper, T. B. Tighe, K. B. Bahnck, H. T. Skriba, M. D. Reinard, B. C. Haynie, R. L. Opila, N. Winograd, D. L. Allara, *J. Am. Chem. Soc.* **2002**, *124*, 5528.
[12] Y. Hirose, A. Kahn, V. Aristov, P. Soukiassian, V. Bulovic, S. R. Forrest, *Phys. Rev. B* **1996**, *54*, 13748.
[13] C. N. Lau, D. R. Stewart, R. S. Williams, M. Bockrath, *Nano Lett.* **2004**, *4*, 569.
[14] M. G. Mason, C. W. Tang, L.-S. Hung, P. Raychaudhuri, J. Madathil, D. J. Giesen, L. Yan, Q. T. Le, Y. Gao, S.-T. Lee, L. S. Liao, L. F. Cheng, W. R. Salaneck, D. A. dos Santos, J. L. Brédas, *J. Appl. Phys.* **2001**, *89*, 2756.
[15] H. Haick, D. Cahen, *Prog. Surf. Sci.* **2008**, *83*, 217.
[16] W. A. de Heer, *Rev. Mod. Phys.* **1993**, *65*, 611.
[17] M. Valden, X. Lai, D. W. Goodman, *Science* **1998**, *281*, 1647.
[18] M. Itoh, V. Kumar, T. Adschiri, Y. Kawazoe, *J. Chem. Phys.* **2009**, *131*, 174510.
[19] W. E. Kaden, T.-P. Wu, W. A. Kunkel, S. L. Anderson, *Science* **2009**, *326*, 826.
[20] S. Duffe, N. Grönhagen, L. Patryarcha, B. Sieben, C. Yin, B. von Issendorff, M. Moseler, H. Hövel, *Nat. Nanotechnol.* **2010**, *5*, 335.
[21] V. Bonačić-Koutecký, L. Češpiva, P. Fantucci, J. Koutecký, *J. Chem. Phys.* **1993**, *98*, 7981.
[22] R. Fournier, *J. Chem. Phys.* **2001**, *115*, 2165.
[23] K. Bromann, C. Félix, H. Brune, W. Harbich, R. Monot, J. Buttet, K. Kern, *Science* **1996**, *274*, 956.
[24] V. N. Popok, I. Barke, E. E. B. Campbell, K.-H. Meiwes-Broer, *Surf. Sci. Rep.* **2011**, *66*, 347.
[25] K. A. Wepasnick, X. Li, T. Mangler, S. Noessner, C. Wolke, M. Grossmann, G. Gantefoer, D. H. Fairbrother, K. H. Bowen, *J. Phys. Chem. C* **2011**, *115*, 12299.
[26] B. Wang, B. Yoon, M. König, Y. Fukamori, F. Esch, U. Heiz, U. Landman, *Nano Lett.* **2012**, *12*, 5907.
[27] G. Yoshikawa, Y. Tsuruma, S. Ikeda, K. Saiki, *Adv. Mater.* **2010**, *22*, 43.
[28] J. E. Reddic, J. C. Robinson, M. A. Duncan, *Chem. Phys. Lett.* **1997**, *279*, 203.
[29] S. T. Shipman, S. Garrett-Roe, P. Szymanski, A. Yang, M. L. Strader, C. B. Harris, *J. Phys. Chem. B* **2006**, *110*, 10002.
[30] M. Nakaya, Y. Kuwahara, M. Aono, T. Nakayama, *Small* **2008**, *4*, 538.
[31] T. Nishikawa, S. Kobayashi, T. Nakanowatari, T. Mitani, T. Shimoda, Y. Kubozono, G. Yamamoto, H. Ishii, M. Niwano, Y. Iwasa, *J. Appl. Phys.* **2005**, *97*, 104509.
[32] M. Kubo, K. Iketaki, T. Kaji, M. Hiramoto, *Appl. Phys. Lett.* **2011**, *98*, 073311.
[33] X. Cheng, Y.-Y. Noh, J. Wang, M. Tello, J. Frisch, R.-P. Blum, A. Vollmer, J. P. Rabe, N. Koch, H. Sirringhaus, *Adv. Funct. Mater.* **2009**, *19*, 2407.
[34] M. S. Dresselhaus, G. Dresselhaus, P. C. Eklund, in *Science of Fullerenes and Carbon Nanotubes*, Academic Press: San Diego, CA **1996**, pp. 224–263.
[35] K. Sakamoto, M. Harada, D. Kondo, A. Kimura, A. Kakizaki, S. Suto, *Phys. Rev. B* **1998**, *58*, 13951.
[36] A. Dodabalapur, L. Torsi, H. E. Katz, *Science* **1995**, *268*, 270.
[37] X. H. Lu, M. Grobis, K. H. Khoo, S. G. Louie, M. F. Crommie, *Phys. Rev. B* **2004**, *70*, 115418.
[38] J. A. Theobald, N. S. Oxtoby, M. A. Phillips, N. R. Champness, P. H. Beton, *Nature* **2003**, *424*, 1029.

© 2013 WILEY-VCH Verlag GmbH & Co. KGaA, Weinheim

[39] E. Mena-Osteritz, P. Bäuerle, *Adv. Mater.* **2006**, *18*, 447.
[40] B. Xu, C. Tao, E. D. Williams, J. E. Reutt-Robey, *J. Am. Chem. Soc.* **2006**, *128*, 8493.
[41] A. Kiebele, D. Bonifazi, F. Cheng, M. Stöhr, F. Diederich, T. Jung, H. Spillmann, *ChemPhysChem* **2006**, *7*, 1462.
[42] S. Yoshimoto, E. Tsutsumi, R. Narita, Y. Murata, M. Murata, K. Fujiwara, K. Komatsu, O. Ito, K. Itaya, *J. Am. Chem. Soc.* **2007**, *129*, 4366.
[43] D. Bonifazi, A. Kiebele, M. Stöhr, F. Cheng, T. Jung, F. Diederich, H. Spillmann, *Adv. Funct. Mater.* **2007**, *17*, 1051.
[44] A. T. N'Diaye, S. Bleikamp, P. J. Feibelman, T. Michely, *Phys. Rev. Lett.* **2006**, *97*, 215501.
[45] S. B. Darling, N. A. Yufa, A. L. Cisse, S. D. Bader, S. J. Sibener, *Adv. Mater.* **2005**, *17*, 2446.
[46] S. A. Claridge, A. W. Castleman Jr., S. N. Khanna, C. B. Murray, A. Sen, P. S. Weiss, *ACS Nano* **2009**, *3*, 244.
[47] I. Horcas, R. Fernández, J. M. Gómez-Rodríguez, J. Colchero, J. Gómez-Herrero, A. M. Baro, *Rev. Sci. Instrum.* **2007**, *78*, 013705.
[48] K. Eichkorn, F. Weigend, O. Treutler, R. Ahlrichs, *Theor. Chem. Acc.* **1997**, *97*, 119.
[49] A. D. Becke, *Phys. Rev. A* **1988**, *38*, 3098.
[50] J. P. Perdew, *Phys. Rev. B* **1986**, *33*, 8822.
[51] TURBOMOLE V6.4 2012, a development of University of Karlsruhe and Forschungszentrum Karlsruhe GmbH, 1989–2007, TURBOMOLE GmbH, since 2007; available from http://www.turbomole.com.
[52] A. Schäfer, H. Horn, R. Ahlrichs, *J. Chem. Phys.* **1992**, *97*, 2571.
[53] D. Andrae, U. Häußermann, M. Dolg, H. Stoll, H. Preuß, *Theor. Chim. Acta* **1990**, *77*, 123.

© 2013 WILEY-VCH Verlag GmbH & Co. KGaA, Weinheim